



Automated defect and contaminant inspection of HVAC duct[☆]



Yongxiong Wang^a, Jianbo Su^{b,*}

^a Key Laboratory of Modern Optical System, and Engineering Research Center of Optical Instrument and System, Ministry of Education, University of Shanghai for Science Technology, 200093 Shanghai, China

^b Department of Automation, Shanghai Jiaotong University, Shanghai 200240, China

ARTICLE INFO

Article history:

Accepted 2 February 2014

Available online 22 February 2014

Keywords:

Ductwork inspection
Imbalance distribution
Seeded k-means
C4.5
Tabu search

ABSTRACT

To sustain acceptable indoor air quality in a building, it is essential to frequently inspect and clean the Heating, Ventilation and Air-Conditioning (HVAC) ductwork. Nowadays the condition inspection is mostly conducted manually according to the video acquired by a pipeline robot. This situation has been significantly resulting in subjectivity, high-cost and inefficiency for HVAC ductwork cleaning and maintenance.

In this paper an automatic defect and contaminant inspection system of HVAC duct is developed. The system consists of an infrared-CCD diagnosis device and a novel supervised method for duct inspection by cascading seeded k-means and C4.5 decision tree. The seeded k-means feature-clustering method first partitions the features of training instances into k clusters using Euclidean distance similarity. C4.5 decision tree is then used to refine the decision boundaries by learning the subgroups within the cluster. Finally the decisions of the k-means and C4.5 methods are combined to achieve the inspection results. To improve the classification performance on the minority classes as well as reduce the computation load during the process, Tabu search is employed for the feature selection and the cost-sensitive function is introduced into Tabu search. Experimental results on real-world data sets demonstrate that the proposed system is effective and efficient in inspecting the condition of HVAC ductwork.

© 2014 Elsevier B.V. All rights reserved.

1. Introduction

By 2009, the total length of HVAC ductwork systems in commercial, healthcare, and school buildings in Shanghai, China had exceeded 15,000 km [1]. Such HVAC ductwork systems in a building are a source of contaminants introduced into occupied spaces. To reduce or eliminate contaminant introduction, properly performing inspection and cleaning services of the systems become necessary. According to the standard of National Air Duct Cleaners Association (NADCA) in the U.S., the recommended inspection frequencies for HVAC systems are likely 1 or 2 years [2]. However the ductwork systems are usually installed below the ceiling of buildings and have many bends and branched ducts, it is very difficult to frequently inspect and clean the ductwork only by manual work. Similar research has been addressed on sewer inspection and its application needs [3–7], there are a few of commercial or testing inspection systems for HVAC ductwork [8]. Among these existing systems, the sewer inspection systems were developed based on a mobile robot (e.g. pipeline robot) equipped with a Closed Circuit Television (CCTV) sub-system. In most cases, when the pipeline robot goes through the ducts, the videos or digital images from the CCTV are gathered and saved in storage system. The off-line

or online inspection is then manually conducted by trained and certified inspectors. Such manual inspection of duct condition has a number of drawbacks including subjectivity, varying standards, high costs and low efficiency. As a result, an automatic condition inspection system is required to improve accuracy, efficiency and economy of the duct inspection work.

The goal of our research work is to develop a portable and automatic defect and contaminant inspection system installed on pipeline robot. The inspection system is capable of automatically detecting defect and assessing contaminants based on visual feedback of the mounted CCTV system.

Duct condition detection is a difficult classification problem because of complex ductwork background patterns, irregularly corroded areas, settled dust, and lack of objective criteria. Some physical defects may be camouflaged in the backgrounds of corroded areas or settled dust. The physical defects and contamination levels are specified by vague terms and attributes, this usually results in variations in manually labeling by experts due to lack of objective criteria, further causing a problem in the interpretation of duct condition in an image. In addition, the duct environments and physical image can often vary from lighting condition etc. These may cause the segmentation method to identify wrong regions of interest (ROI). In summary, all of these issues complicate the task of duct inspection. So far it is hard to find reliable and robust features to accurately assess the duct condition.

[☆] Supported by the National Science Foundation of China (No. 61221003).

* Corresponding author. Tel./fax: +86 21 34204276.

E-mail address: jbsu@sjtu.edu.cn (J. Su).

The ducts should be classified into three classes: normal ducts, contaminated ducts, and physical defect ducts based on the purpose of cleaning and restoration [2]. In this work, we propose a novel approach based on seeded k-means feature-clustering and C4.5 decision tree to perform automatic inspection and assessment of duct condition. The decisions of combining seeded k-means and C4.5 methods are used to achieve the inspection results. To improve real-time as well as the detection performance on minority class, we focus on two main problems: feature selection and imbalance data distribution, which need to be improved in anomaly or defect detection. Tabu search (TS) with cost-sensitive function is employed for feature selection. Combining k-means and the C4.5 is used to relieve imbalance data distribution and acquire high performance in defect and contaminant detection of an HVAC duct. Meanwhile, the inspected 3-D interior surface of the duct can be reconstructed in real time for the assessment.

The rest of this paper is organized as follows. Section 2 provides a literature review about the related work. Section 3 describes the proposed systematic methodology which includes feature extraction, feature selection by the proposed Tabu search and cascading detection algorithm. The experimental setup and results are presented in Section 4. Section 5 concludes the work.

2. Reviews on pipeline inspection technology and associated methodologies

Currently there are rarely available technologies for automated condition inspection of HVAC ducts. Alternatively, due to technical and methodological similarities, we review the existing pipeline inspection technologies, defective surface inspection methodologies, and associated machine learning methods.

The major technologies applicable to the pipeline inspection are as follows: Closed-Circuit Television (CCTV), ultrasonic, laser, Infra-Red thermography, and so on [9]. Pipeline inspection systems based on CCTV or digital images include an early multi-sensory robotic system called KARO [3], and Pipe Inspection Real-Time Assessment Technique (PIRAT) [4]. Pipe detection techniques based on laser profiling [6] and ultrasonic profiling [10] are implemented to inspect sewer and oil pipelines recently. In Ref. [11], the Ground Penetrating Radar (GPR) and Digital Scanning and Evaluation Technology (DSET) are reported, which are utilized to collect accurate information about the condition of a buried pipeline. There are some similarities between pipeline inspection and HVAC duct inspection, such as similar working conditions and the objectives of inspecting physical defects. However, one of main purposes of HVAC duct inspection is detecting surface contaminants and deposits unlike pipeline inspection. Thus pipe detection techniques based on laser profiling, ultrasonic profiling, and so on are not suitable for HVAC duct inspection. In these technologies, the methods based on CCTV videos and digital images can provide much more visualized pipeline information. The visual information can be used by inspectors during and after the pipe inspections and can be easily fused with other sensor data. As a result, the technology based on digital images is currently one of the most popular technologies for HVAC duct inspection. The methods of anomaly detection or surface defect inspection via images can be applied to HVAC duct inspection.

Anomaly detection or surface defect inspection via images [12] developed using machine learning techniques like artificial neural networks [5,6], radial basis network [12], decision tree [14], SVM, and others [12] have become popular because of their high detection accuracies at low false positive rates. However, the anomaly detection related studies cited above have two problems which need to be improved: 1) Feature selection should be carried out to reduce the cost of extracting features and improve the classification accuracy. 2) The imbalance data distributions in anomaly or defect detection are often neglected. Generally, the classifier often tends to

recognize new samples as the majority class without reducing the total recognition rate, so the classification precision to the minority class is very low. There are many cases where a small imbalance may be very harmful in difficult-to-learn tasks with overlapping classes and/or in the absence of a sufficient number of training points [15]. HVAC duct inspection is done to recognize the anomalous ducts which are rare. Thus, class imbalance is a very important issue in anomaly detection for an HVAC duct.

The approaches of feature selection can be classified into filter, wrapper, and sub-optimal searching and optimal searching approaches [15]. Among them, Tabu search has proved to be a promising technique for feature selection with respect to the quality of the obtained feature subset and computation efficiency [16]. In refs. [16,17], it has been shown that not only could Tabu search obtain the optimal or near-optimal solution, it also required less computational effort than other suboptimal and genetic algorithm based methods. The integration of neighborhood, memories, aspiration criteria, tabu moves, and diversification strategies makes TS more effective and more complicated than classical feature search algorithms. However, they did not take into account the problem of unbalanced data distribution. To cope with imbalance data, a number of approaches have been proposed, which evolve along four major directions [15]: 1) Data-level approaches, such as oversampling of the small class or undersampling of the large class; 2) cost-sensitive approaches, one way is to use different C parameters in the cost function for the two classes in classifiers; 3) feature selection; and 4) ensemble, fusion, and cascading of multiple machine learning methods that have a better performance yield over individual methods [13].

In view of the diversities of feature distributions within a class, we can preprocess the data to employ the clustering algorithms like k-means, SOM, fuzzy C-mean and so on. The significance of clustering in an image has been highlighted in Ref. [16]. It is particularly in cases where there are several categories of defect sub-classes corresponding to severity and physical manifestation. We choose seeded k-means [18] for clustering because: 1) it is a data-driven method with relatively few assumptions on the distributions of the underlying data and 2) the greedy search strategy of k-means guarantees at least a local minimum of the criterion function, thereby accelerating the convergence of clusters on large data sets. However, the data distributions in defect inspection are unbalanced and noisy, which will give rise to 1) the class dominance problem when the training data have a large number of instances from one particular class and very few instances from the remaining classes, and 2) the forced assignment problem when the k parameter in k-means is set to a value that is considerably less than the inherent number of natural groupings within the training data [13]. The two problems would result in high detection error and even misclassification of the total minority class. In Ref. [13], cascading k-means clustering and the ID3 decision tree is used to relieve the two problems and acquire high performance in anomaly detection. However, earlier ID3 has some weaknesses which need to be improved. C4.5 made a number of improvements to ID3, for example, C4.5 can handle continuous features, training data with missing attribute values, and attributes with differing costs. Its splitting criterion is the normalized information gain unlike ID3.

Our work is inspired by the research work in Ref. [13,16,18]. That is, the seeded k-means feature-clustering method is used to first partition the training instances into k clusters, then a C4.5 works on the output from the clustering algorithms. The weighted combining decision of k-means and C4.5 is finally applied to achieve the final decision of classification. The best weighting value of combining decision of k-means and C4.5 is acquired by TS. Note that, to relieve the imbalance data distributions, we construct new sample sets by using oversampling and undersampling, and introduce the cost-sensitive function in TS to alleviate the unbalanced situation by emphasizing the importance of high recognition rate of the minority class in the process of feature selection.

3. The proposed systematic methodology

3.1. System architecture

The proposed systematic architecture for automated duct inspection consists of the integrated methods of pre-processing, segmentation and feature extraction, clustering using k-means feature-clustering, C4.5 decision tree, interpretation by combining k-means and C4.5, and 3-D reconstruction and feature selection during the training phase. The schematic diagram is shown in Fig. 1. Following the diagram, the high resolution 2-D image of the duct is captured by a digital camera. After preprocessing the image and image segmentation, some geometric features, statistical features and features in frequency domain from the ROI of the image are extracted for the duct condition assessment. The k-means feature-clustering algorithm partitions the feature space into k disjoint clusters and computes centroids of k clusters. A C4.5 is then employed for classifying the image to k classes. The final interpretation (assessment) of duct condition will be made based on results of weighted combining the k-means clustering and C4.5 classification. In the training phase, the features and the best weight of combining classifiers are selected by Tabu search with the cost-sensitive function in order to reduce the computation complexity and improve the performance of detection. The digital images and features can be displayed by a Graphic User Interface (GUI) in real time. Meanwhile, the 2-D surface texture image will be recovered to be the 3-D surface texture map that is displayed in the GUI.

3.2. Segmentation and feature extraction

Several typical duct images are shown in Fig. 2. Due to the rust and the long-term settled dust, the detected objects may have a similar color as the dust background. Some defects are camouflaged in the corroded areas or settled dust. The raw image filtering and imagery enhancement will be the first step of the work before the image segmentation.

3.2.1. Image Segmentation

The edge detection methods can greatly reduce the amount of the information in the case of keeping the shape features and segmented ROI in an image. There are many commonly used edge detection approaches, such as morphology methodology [19], Otsu's technique [14], and Canny edge detection. In the application of pipeline inspection, the geometrical edges can be effectively segmented by using the morphology methodology [14,19]. However, in the application of duct inspection, due to the extreme background noise and dirt of the duct surface, the optimum segmentation parameters vary considerably

from one image to another. So some common edge detection methods may not be applicable. We adopt a level set based on the Chan–Vese model (CV) [20] to segment the original image and gain the piecewise smooth edge. The CV model, which is the active contour to detect objects in a given image, has the ability of detecting smooth boundaries, scale adaptation, automatic change of topology, and robustness with respect to noise. The approach is based on techniques of curve evolution, Mumford–Shah functional for segmentation and level sets. The optimal partition problem is solved by minimizing the following energy functional [20]:

$$F(C, c_I, c_O) = \int_{\text{inside}(C)} (u(x,y) - c_I)^2 dx dy + \int_{\text{outside}(C)} (u(x,y) - c_O)^2 dx dy, \quad (1)$$

where $u(x, y)$ is the gray value of image pixel (x, y) , c_I is the average value of the gray inside contour C , c_O is the average value of the brightness outside contour C . Generally, the level set of the CV model needs to manually set the initial curve [20]. In this paper, the closed edge acquired from image segmentation by Otsu's method is set as the initial curve C of the level set, such that the automatic setting initial values are achieved.

3.2.2. Feature extraction

After SUSAN edge detection, the mathematical morphological operation is used to remove the noise and acquire the closed edge curves. To select features by using TS, we extract enough features from duct images, such as geometrical features, features from gray level co-occurrence matrix, wavelet-based features, LBP, and other features describing the roughness, density, shape, etc.

A Geometrical features

We adopt the following simple scalar region descriptors to represent other shape features besides the area, width and length in our work:

- (1) Compactness: Compactness is a popular shape description characteristic independent of linear transformations given by [21]

$$\text{Compactness} = \frac{(\text{region_border_length})^2}{\text{area}}. \quad (2)$$

The most compact region in a Euclidean space is a circle. Using the outer boundary, compactness assumes values in the interval $[16, \infty)$ [21]. The compactness of the hole equals that of a circle approximately. The compactness of other shape objects, such as joints and cracks, is apparently larger than that of the hole.

- (2) Eccentricity: The simplest eccentricity characteristic is the ratio of the major to the minor axes of an object [21]. Obviously, the linear shape objects like joints and cracks have the largest eccentricity. The eccentricity of the hole is only slightly larger than 1.
- (3) Convexness. Let u represent a set of contour points obtained from level set and its convex hull (denoted as $C(u)$). The convexity measure is defined as $C_c(u) = \text{Area}(u) / \text{Area}(C(u))$.
- (4) Moment invariants: Moments are extensively used for shape representation and pattern recognition, which makes them a very useful feature set to include [22]. The seven moment invariants that are first introduced by Hu in Ref. [22] are used.

B Statistics features

- (1) Gray histogram

The gray histogram is a first-order statistics feature which acts as a graphical representation of the intensity distribution in a digital image. It plots the number of pixels for each intensity value and is shown in the GUI.

- (2) Surface roughness

Surface roughness is used widely in the industry and is generally used to quantify the smoothness of a surface finish or surface texture. The arithmetic mean deviation of surface profile R_a is

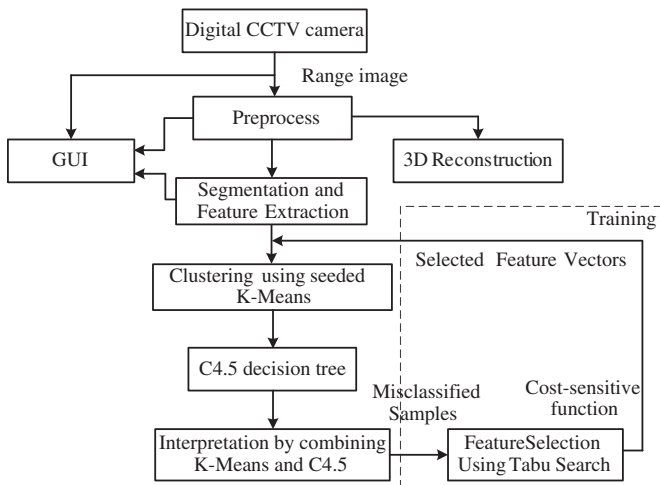


Fig. 1. Schematic diagram of the inspection system.

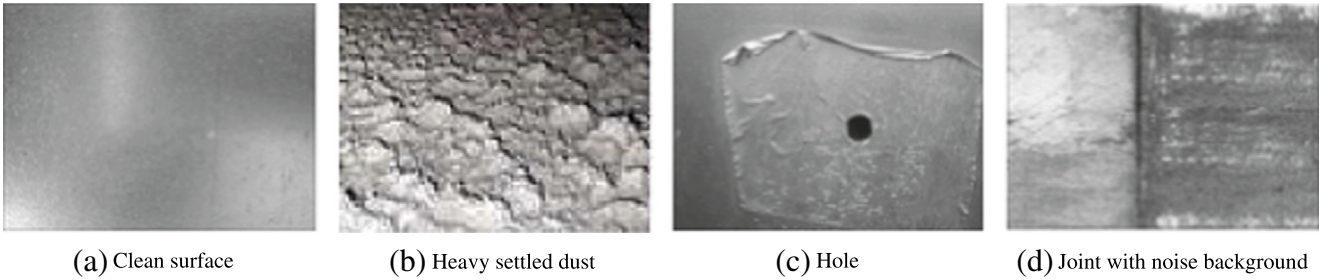


Fig. 2. Typical HVAC duct images.

universally recognized and can be defined as a critical feature of surface roughness in ducts. Luk [23] proposed an approach to measuring the surface roughness based on images. The roughness is defined as the ratio between the standard deviation of the image gray-scale and the root mean square height of the gray-level distribution along the row axis or column axis. More reasonably, we used a modified formula to achieve only one roughness average for full representation of duct surface roughness. The modified method is based on the polar-coordinate scanning. Instead of scanning along X and Y coordinates, it now performs a circular scanning in the polar coordinate. The center of the image acts as the original point of the polar coordinate. We then calculate the aggregate of roughness R_a of each rotationally scanned profile according to the rotation angle, γ . Then the new defined R_a is given by:

$$R_a|_{a=\gamma} = \left(\frac{\frac{1}{N-1} \sum_{i=0}^{l-2} n_i (i-\mu)^2}{\frac{1}{N} \sum_{i=0}^{l-1} n_i^2} \right)^{1/2}, \quad (3)$$

where

$$N = \sum_{i=0}^{l-1} n_i, \mu = \frac{1}{N} \sum_{i=0}^{l-1} i \cdot n_i, \quad (4)$$

where n_i denotes the number of pixels whose gray scale is i at γ angle, and l is the gray-scale number. When it scans 360° , the surface roughness of the whole image can be computed and displayed in the GUI. In Ref. [24], the results from the previous work agree with those done by Luk's method.

(3) Co-occurrence matrices

The gray level co-occurrence matrix $p_{ij}(\theta, s)$, which have been widely used in texture classification or texture segmentation [21], is defined as the probability of pixels i and j with a specified distance of s and direction of θ occurring in the image. Generally, there are 14 types of co-occurrence features derived from co-occurrence matrices useful for pattern classification. However, the relationship between the co-occurrence features is not absolutely independent so that the redundant features would reduce the efficiency of pattern classification. Through a discriminant analysis, the most independent co-occurrence features with correlation coefficients of less than 0.5 were found as entropy (*Entro*), correlation (*Corre*), and cluster tendency (*Clust*) [14]. In this paper, three features have been chosen to describe the texture of in the HVAC duct images:

$$Entro = - \sum_{i=1}^n \sum_{j=1}^n P_{ij} \cdot \log P_{ij}, \quad (5)$$

$$Corre = \frac{\sum_{i=1}^n \sum_{j=1}^n (i \cdot j) P_{ij} - \mu_x \mu_y}{\sigma_x \sigma_y}, \quad (6)$$

$$Clust = \sum_{i=1}^n \sum_{j=1}^n (i - \mu_x + j - \mu_y)^2 \cdot P_{ij}, \quad (7)$$

where

$$P_{ij} = \frac{M_{ij}}{\sum_{i=1}^n \sum_{j=1}^n M_{ij}}, \mu_x = \sum_{i=1}^n \sum_{j=1}^n i \cdot P_{ij}, \mu_y = \sum_{i=1}^n \sum_{j=1}^n j \cdot P_{ij}, \quad (8)$$

$$\sigma_x = \sqrt{\sum_{i=1}^n \sum_{j=1}^n (i - \mu_x)^2 \cdot P_{ij}}, \sigma_y = \sqrt{\sum_{i=1}^n \sum_{j=1}^n (j - \mu_y)^2 \cdot P_{ij}}. \quad (9)$$

Co-occurrence features are affected by the distance and the direction between the two pixel positions mainly and the gray scale quantization levels are not important in the general case. The distance and direction between the two adjacent pixels have the inherent discipline and they do not change the feature value ratio between different textures. In this paper, the distance $s = 1$ and the direction $\theta = 0^\circ, 45^\circ, 90^\circ$, and 135° are chosen.

(4) Wavelet-based features

Wavelet-based features can extract the information in the frequency domain, and their effectiveness in performing the texture analysis has been proved [24]. The subbands of the digital images are generated by using the discrete wavelet transform (DWT) [25]. Within each subband, the following features are calculated [24]:

$$f_1(l, q) = \frac{1}{A} \sum_j \sum_j |I_{i,j}(l, q)|, \quad (10)$$

$$f_2(l, q) = - \frac{1}{\log A} \sum_j \sum_j \frac{|I_{i,j}(l, q)|}{N} \log \left(\frac{|I_{i,j}(l, q)|}{N} \right), \quad (11)$$

where $N = \sum_{i,j} |I_{i,j}(l, q)|$, l represents the decomposition level, q is the subband number within the decomposition level l , and A is the area of each subband. The feature $f_1(l, q)$ represents the amount of signal energy at a resolution, and feature $f_2(l, q)$ shows the non-uniformity of the subband values. In our paper, a wavelet transform with three levels is adopted.

(5) Local binary patterns (LBP)

The LBP operator [26] is originally designed for texture description. It is a robust but theoretically and computationally simple approach. It combines the separate statistical and structural approaches to texture analysis by simultaneously analysis of both stochastic microtextures and deterministic macrotextures. In addition, it has shown excellent performance in many comparative studies.

A form of the local texture T is defined as $T \approx t(s(g_0 - g_c), \dots, s(g_{p-1} - g_c))$, where g_c is the gray value of the center

pixel of a local neighborhood. g_p is the gray value of the p th symmetric neighborhood pixel in a circle of radius R . If $x \geq 0$, $s(x) = 1$, otherwise, $s(x) = 0$. For simplicity, we just choose $p = 8$, $R = 1$ in this paper. As an extension of the LBP operator which is called “uniform” patterns, the numbers of transitions or discontinuities in the circular presentation of the pattern are computed [26]. Then, the discrete occurrence histogram of the “uniform” patterns is computed over an image or a region of an image as a texture feature.

3.3. 3-D texture re-construction

“Shape from shading” methods [27] are implemented to recover the 3-D texture map from the 2-D surface image of the duct. Assume that the gray value of the image is linear with respect to the surface radiosity, and then we could find the relationship between image intensity $I_p(x, y)$ and surface normal $N(x, y)$. Eq. (12) gives the relationship between surface normals and a parameterized equation of the surface which can be used to generate a mesh to reconstruct the geometry of the object.

$$N(x, y) = \frac{\mathbf{g}(x, y)}{\|\mathbf{g}(x, y)\|_2} = \frac{1}{\sqrt{1 + \frac{\partial f^2}{\partial x^2} + \frac{\partial f^2}{\partial y^2}}} \left[-\frac{\partial f}{\partial x} \quad -\frac{\partial f}{\partial y} \quad 1 \right]^T, \quad (12)$$

where $\mathbf{g}(x, y)$ is the surface vector, $f(x, y)$ is the equation for the parameterized surface which can then be integrated over x and y to yield the final model. Consider that the graph of $f(x, y) = xy$, which is linear in both the x and y directions. If we assume that the value of the unit normal at some point (x, y) is $(a(x, y), b(x, y), c(x, y))$ and the depth $z(x, y)$ is the function of the surface, then it is easy to have that:

$$\frac{\partial z}{\partial x} = \frac{-a(x, y)}{c(x, y)} \quad \text{and} \quad \frac{\partial z}{\partial y} = \frac{-b(x, y)}{c(x, y)}. \quad (13)$$

If we assume that the z -value at the reference point is 0, the z -value at any other point will be an integral of $(\partial z / \partial x, \partial z / \partial y)$ [27] along some paths. From above approaches, the 3-D surface texture map can be reconstructed. Obviously, the recovered 3-D surface texture provides more clear and complete information to characterize the duct surface texture. According to the 3-D map, roughness and edge detection map, operators can easily and completely assess the inner condition of the duct.

3.4. Feature selection based on Tabu search

Feature selection is a dimensionality reduction problem in order to reduce measurement costs, shorten computational time, relieve the curse of dimensionality, and improve classification accuracy [15]. The unsupervised clustering algorithms such as k -means are sensitive to irrelevant features and noise. Therefore feature selection can improve the performance of clustering as reported in Ref. [16]. Our objective of employing Tabu search is to find an optimal subset having a predefined number of features to yield the lowest error rate of the classifier. The Tabu search flow chart is shown in Fig. 3.

An example of initial solution is shown in Fig. 4. The TS begins from a predefined number of features. 0 indicates that the feature is not included in the solution while 1 indicates that it is. The initial weight of combining classifier is set as 0.5. The weight values range from 0 to 1, and its step size is 0.1, i.e. $\alpha \in [0, 1]$.

In Refs. [16] and [17], the cost function is defined as

$$Cost = \sum_{i=1}^n C_i \cdot NE_i, \quad (14)$$

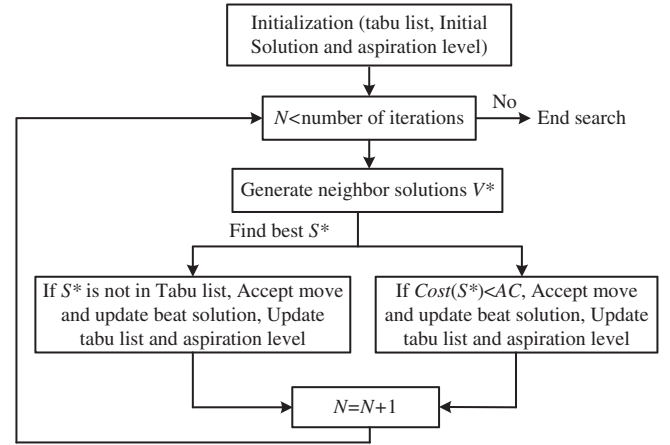


Fig. 3. Algorithmic flow chart of TS.

where n is the number of classes, C_i is the misclassification cost for each sample in the i th class. NE_i is the total number of misclassified samples for the i th class. They did not differentiate between the majority class and the minority class in cost function. Our objective function aims to minimize the error rate of minority class in the context of the classification accuracy of majority class being acceptable. So we add cost sensitivity of imbalance distributions into the cost function as given in Eq. (15).

$$Cost = \sum_{i=1}^n C_i \cdot \frac{NE_i}{N_i}, \quad (15)$$

where N_i is the total number of samples in the i th class.

From Eq. (15), it can be seen that the lesser the total number of samples in minority class, the bigger the cost value, such that Tabu search emphasizes the importance of achieving high recognition rate of minority class. During each iteration, neighbors are generated by randomly adding and deleting a feature from the feature vector of size n . Among the neighbors, $10M^n$ neighborhood solutions are then evaluated using Eq. (15) and the one with the best cost, i.e. the solution results in the minimum value of Eq. (15), is selected and adopted as a new current solution for the next iteration. The initial standard parameters of Tabu Search are: $N = T = \sqrt{F}$ [16], where N is the number of neighborhood solutions, T is the size of Tabu list and F is the number of features. The size of Tabu list can be determined by experiments. There is an occurrence of cycling when the size is too small, and there is a deterioration of solution quality when the size is too large. The termination condition is the set number of iterations. For more details refer to Ref. [16].

3.5. Duct condition inspection using seeded k -means feature-clustering and C4.5 algorithm

3.5.1. Anomaly detection with seeded k -means feature-clustering

Although all duct samples are artificially classified into k typical classes according to their severity and appearance, the diversities of feature distributions within each class are not addressed. The class of contaminated ducts and physical defect ducts include many subclasses such as

F_1	F_2	\dots	F_n	α
1	1	\dots	0	0.5

Fig. 4. The structure of the encoding scheme used in TS and an example of the initial solution.

debris, rust, hole and crack. There usually exist large differences between their feature distributions and some overlaps within the same subclasses. We first combine the selected features as a one-dimensional feature vector for feature clustering. We then employ the feature-clustering approach, seeded k-means [18], to preliminarily classify these features within the classes.

In many cases, knowledge of the relevant classification is incomplete. The semi-supervised clustering can group data using labeled data to generate seed clusters that initialize a clustering algorithm. Proper seeding biases clustering towards a good region of the search space, thereby it can reduce the effects from irrelevant features and noises in unsupervised clustering. In the seeded k-means, the seed cluster is only used for the initialization. The steps in the seeded k-means-based duct detection are as follows:

1. Initialize k cluster centers, r_h , using the mean of l th in the seed set according to supervision, for $h = 1, \dots, k$. (We assume that there is at least one seed point that belongs to each class.)
2. Assign cluster: Assign each data point x to the nearest cluster h , for $h = \arg \min \|x - r_h\|^2$.
3. Update each cluster center r_h as the mean of all data that belongs to it.
4. Repeat steps 2–4 until cluster centers are stable.
5. For each test sample Z :
 - a. Compute the distance $D(r_i, Z)$, $i = 1, \dots, k$, find the cluster r_i that is closest to Z .
 - b. Classify Z using either the threshold rule or the Bayes decision rule.

The threshold rule: Assign $Z \rightarrow 1$ (Z belongs to the cluster r_i) if $P(\omega_l = 1|Z \in C_i) > \tau$, and τ is a threshold; otherwise $Z \rightarrow 0$, where “0” and “1” represent normal and anomaly class, respectively. ω_l represents the anomaly class in the cluster r_i , and $P(\omega_l = 1|Z \in C_i)$ represents the probability of anomaly samples in r_i .

The Bayes decision rule: Assign $Z \rightarrow 1$ (Z belongs to the cluster r_i) if $P(\omega_l = 1|Z \in C_i) > P(\omega_l = 0|Z \in C_i)$; otherwise $Z \rightarrow 0$, where ω_l represents the anomaly class in the cluster r_i , and $P(\omega_l = 0|Z \in C_i)$ represents the probability of normal samples in r_i .

3.5.2. Anomaly detection with C4.5 decision tree

C4.5 decision tree is an extension of the ID3 algorithm to address some issues not dealt with by ID3, such as avoiding overfitting the data, reduced error pruning, handling continuous attributes, and so on. C4.5 builds decision trees from a set of training data using the concept of information gain ratio in the same way as ID3. The information gain ratio on each attribute A , is defined as

$$\text{GainRatio}(S, A) = \frac{\text{Gain}(S, A)}{-\sum_{i=1}^c p_i \log_2(P_i)} \quad (16)$$

where S is the total input space, $\text{Gain}(S, A)$ is information gain on attribute A as ID3. p_i represents the probability of class “ i ”. The attribute with the highest information gain ratio, say B , is chosen as the root node of the tree. Next, a new decision tree is recursively constructed over each value of B using the training subspace $S - \{S_B\}$. A leaf-node or a decision-node is formed when all the instances within the available

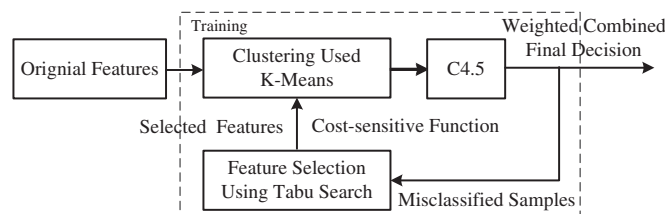


Fig. 5. The diagram of the proposed seeded k-means/C4.5 detection algorithm.

training subspace are from the same class [13]. For duct anomaly detection, the C4.5 decision tree outputs the probability of belonging to a class.

3.5.3. Seeded k-means/C4.5 classification algorithm for duct condition assessment

The seeded k-means/C4.5 has two steps: 1) training phase and 2) testing phase. During the training phase, the seed set is first assigned to k classes according to the supervision, as shown in Fig. 5. Then the feature-clustering method is used to partition the training space into k disjoint clusters, C_1, C_2, \dots, C_k and the centroids of C_1, C_2, \dots, C_k are obtained as r_1, r_2, \dots, r_k , respectively. A C4.5 is then built and trained based on the desired outputs. The k-means method ensures that each training instance is associated with only one cluster. However, if there are subgroups or overlaps within a cluster, the C4.5 decision trained on that cluster refines the decision boundaries by partitioning the samples over the feature space.

Given a sample S , the distances d_1, d_2, \dots, d_k between the sample S and the centroids r_1, r_2, \dots, r_k of k clusters are achieved, respectively. For each class, we use the following equation to obtain the final probability.

$$P_l = \alpha \cdot \mu_l + (1 - \alpha) \cdot D_l \cdot P(\omega_l = 1|Z \in C_l), l = 1, \dots, n, \quad (17)$$

$$\text{where } D_l = 1 - \frac{d_l}{\sum_{i=1}^k d_i}$$

where D_l is the scale factor of Euclidean distance, $\mu_l \in (0, 1)$ is the C4.5 output for the l th class, and n is the number of anomaly samples classified into the l th class in k-means. α is the combining weighted value and is determined by TS. The final detection results are acquired by using the threshold rule. The feedback and the misclassified samples from the final classification results allow the Tabu search to iteratively search for the feature vectors that can improve the classification accuracy. In the testing phase, only k-means/C4.5 is used to classify the instance.

4. Experiments

4.1. Experimental setup

4.1.1. The sensor prototype for HVAC duct inspection

The sensor system consists of two high resolution CCD cameras that can capture the two-direction duct images by pan and tilt cameras, and the active infrared LED lighting source that produces 1.6 mW 850 nm infrared light. Compared with ultrasonic and laser lighting sources, our system is compact, low cost, and can acquire clear images. The inspection principle of the sensor is illustrated in Fig. 6. The pan and tilt CCD cameras and IR lighting source are fixed at the front end of the robot arm of our pipeline robot. The sensor can capture surrounding images of the duct by rotating 360° around the axis of the robot arm and adjusts the image size by vertical locomotion. If needed, the manipulator of the robot can sample the particles within the duct, and then cleaning

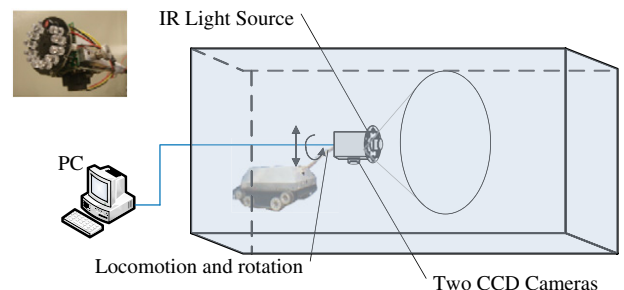


Fig. 6. Schematic diagram of the inspection principle of the sensor.

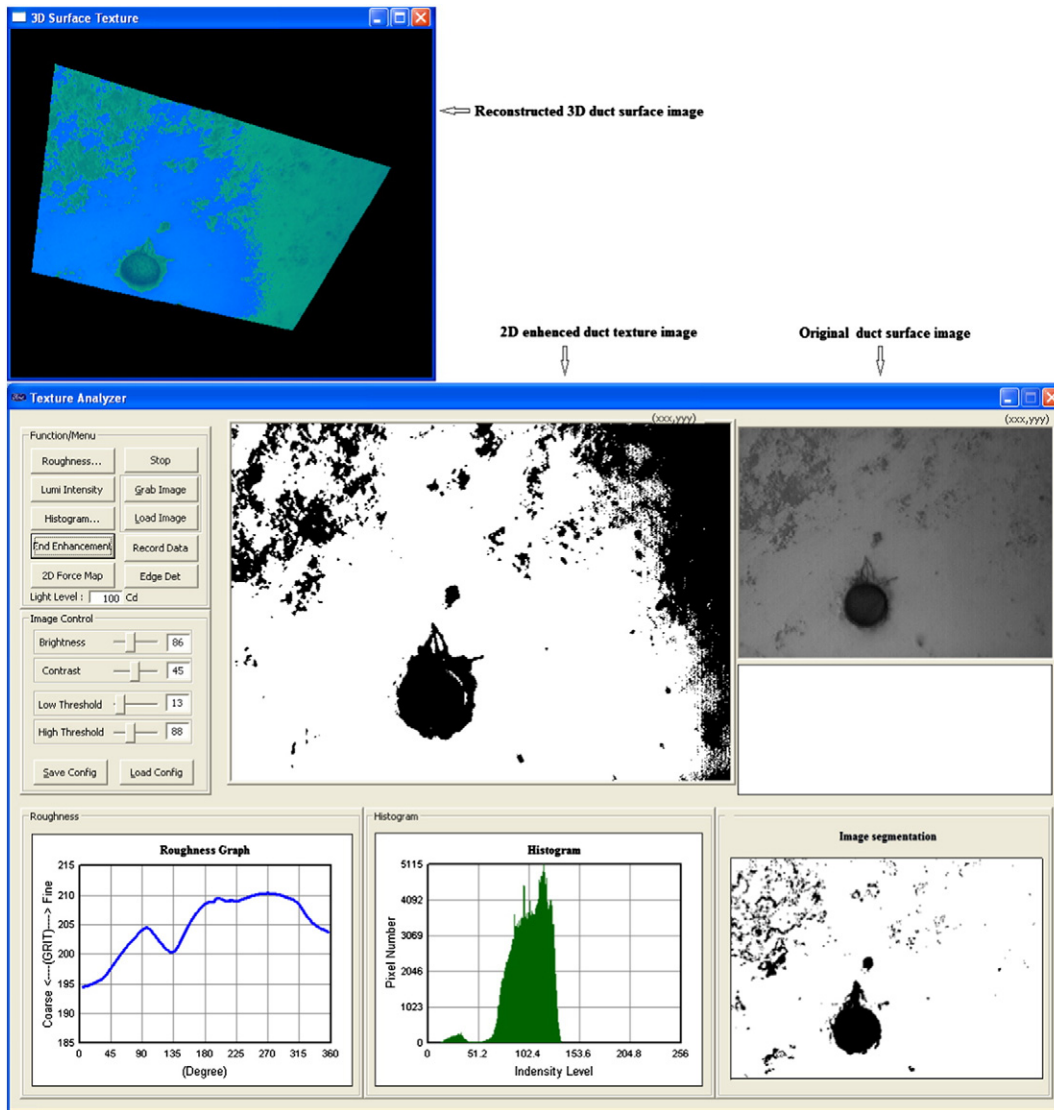


Fig. 7. Snapshot of the GUI interface with a duct image having rust and a hole.

solution and sterilizing fluid will be determined after the assay and analysis of the particles.

4.1.2. Graphic User Interface (GUI)

The operators can remotely control the robot through the visual feedback. The image from the tilt camera is mainly used for the navigation. The image from pan camera is used to segment the image and extract features for the assessment of duct condition. CCTV images, the processed duct images, and the extracted features are displayed in a Graphic User Interface (GUI) in real-time. Fig. 7 is a snapshot of the GUI. As shown in the figure, the GUI contains three characterization windows displaying the roughness graph, histogram graph, and edge detection map, and two image windows. The small image window displays the original image captured from the sensor; the big one shows the enhanced 2-D image after image processing. Associated with three graphs and two image windows, several functional buttons that can

adjust the image contrast, brightness, and threshold online, are shown in the left side of the interface. Using the “shape from shading” methods [27], the re-constructed 3-D surface map from the 2-D image is shown in the top of Fig. 7.

4.2. Image data set

Many HVAC duct images of size 860×780 have been acquired from Shanghai, China. The contaminated ducts and physical defect ducts include some sub-classes. However, it is difficult to acquire enough images of minority classes because of the imbalance distribution of samples. The actual distribution of samples includes about more than 93% clean ducts (majority class), 6% contaminated ducts (settled dust, debris, and so on), and less than 1% physical defect ducts (holes, cracks, gaps and rust). Sampling techniques can correct problems with the imbalance distribution of a data set [15]. Both oversampling of the small class and

Table 1

Sub-image samples of each class.

Sub-images	Clean ducts	Clean ducts with texture	Contamination ducts	Debris	Rust ducts	Gaps and cracks	Holes
Number the samples	263	362	108	78	92	83	5

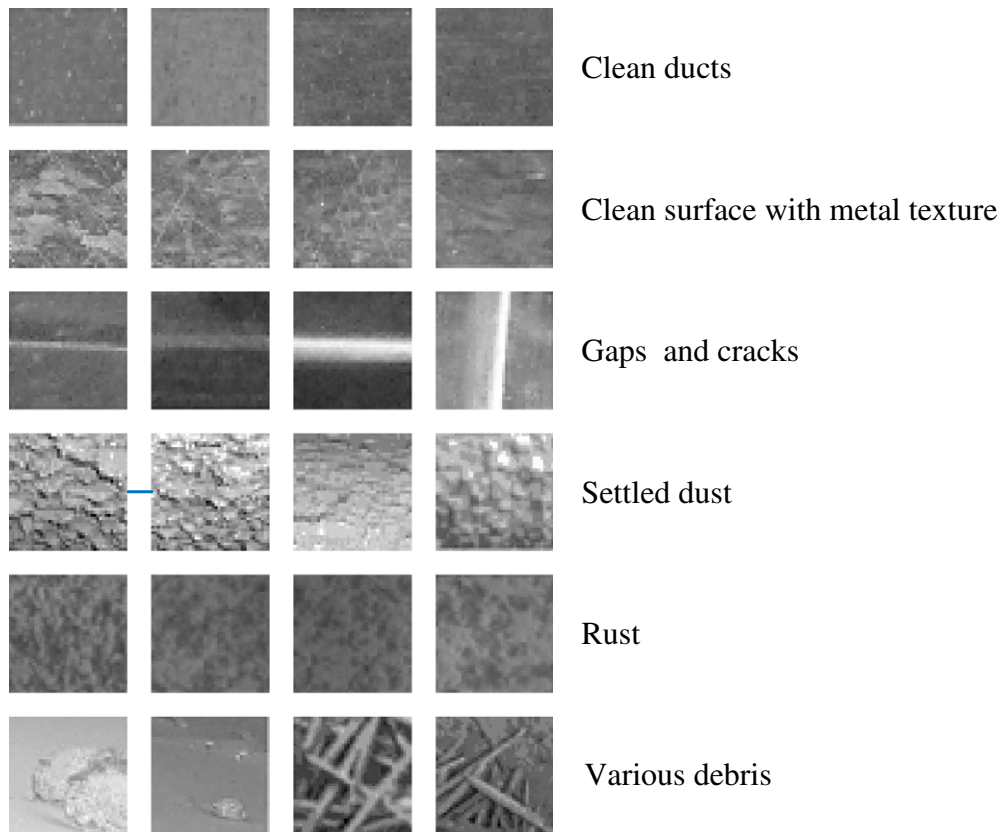


Fig. 8. Typical sub-images of HVAC ducts.

undersampling of the large class are used in our data set. From the above original images, we extract 991 sub-images which include some typical samples, as listed in Table 1. The typical sub-images are shown in Fig. 8. The ducts with both contaminants and physical defects should be classified into physical defect class because the samples of the physical defect class are the least and these ducts need to be restored.

For each sub-image, we extract 102 original features including 13 shape features, 32 features from gray level co-occurrence matrix, 16 wavelet-based features, 36 local binary patterns (LBP), and 5 other features. These features can describe the roughness, density, shape, multi-spectra, and texture of the images.

4.3. Experimental results

4.3.1. Experimental results of image segmentation with the level set method

In our paper, the Otsu's technique is firstly adopted to segment the air duct image. A region-filling algorithm [25] is applied to eliminate

the holes within the segmented regions. Then, the morphological open and close operators with a three-pixel-diameter disk structure element are performed to filter very thin edges and random noise regions, which may be caused by the small debris or color of the background. The level set is lastly used to refine the coarse edges of the duct image. The proposed image segmentation method works very well for duct images as shown in Fig. 9, which represents the processing procedure of our image segmentation method step by step.

4.3.2. Detection experiments based on different feature sets

In our experiment, we just use 5-fold cross validation to the validity of features selection and classification performance because of the deficiency of minority classes. To evaluate the classification performance of the minority classes, the correct rate of detection is defined as follows:

$$Cr(C_i) = \frac{NC(C_i)}{N(C_i)} \times 100\% \quad (19)$$

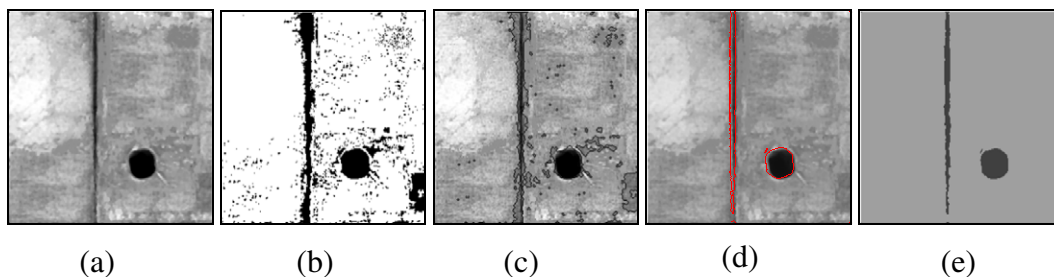


Fig. 9. The final and intermediate results of image segmentation in a typical image sample. (a) Original image. (b) Otsu's segmented image. (c) The image with the coarse edges segmented by Otsu's method. (d) The final segmented image with mixed red curves of CV level set. (e) The final segmented gray-value image by level set.

where $N(C_i)$ is the total number of class C_i , $NC(C_i)$ is the number of correct classification in class C_i . For multi-class problem, a new criterion, total AUC, is introduced in Ref. [28]. In this paper, a separate AUC for each class is firstly calculated, such that the AUC of class C_i is calculated by considering all the samples of class C_i as positives and the samples of all other classes as negatives. Then, the total AUC is calculated as the summation of the AUCs weighted by the class prior probability given as follows:

$$Auc_t = \sum_{C_i} Auc(C_i) \cdot P(C_i), \tag{20}$$

where $Auc(C_i)$ is the AUC of C_i , and $P(C_i)$ is the prior probability of C_i .

1) Detection experiments based on single feature set
 To evaluate the discriminating capability of the features the experiments of anomaly detection using k-means/C4.5 with various feature sets are performed. For the k-means and C4.5 cascading, the value of k was set to 7 according to the appearance of duct images. The experiment aims to compare the classification performance using k-means + C4.5 based on every single feature set, i.e. shape set, wavelet-based features (WBF) set, LBP set, and gray level co-occurrence matrix (GLCM) based feature set. In Fig. 10, the results show that the shape feature set has the worst classification performance, WBF, LBP and GLCM have relatively high performance, and MGDF's worse performance may be due to the instability of the high-frequency component.

2) Detection experiments based on various combined feature sets and Tabu-search selected features

To evaluate the results of feature selection using Tabu search, we conduct a set of experiments using the proposed k-means + C4.5 ensemble classifier based on different combined (by hand) feature sets and the feature sets selected by Tabu search. The results are shown in Fig. 11. From Figs. 10 and 11, it can be seen that the performance using combined feature sets are better than the performance of using the single feature set in duct inspection. The selected feature sets by Tabu search are more suitable for the duct condition inspection than all features. This is because the irrelevant features that “confuse” k-means method are removed by feature selection, and then the seeded k-means algorithm is capable of finding clusters with good quality. The cost-sensitive function of TS is applied to attach more importance to recognition rate of the minority class in the process of feature selection. Fig. 11 clearly demonstrates the significant improvement in correct rates of detection for minority classes (2nd and 3rd) based on the selected feature using the Tabu search with cost-sensitive function.

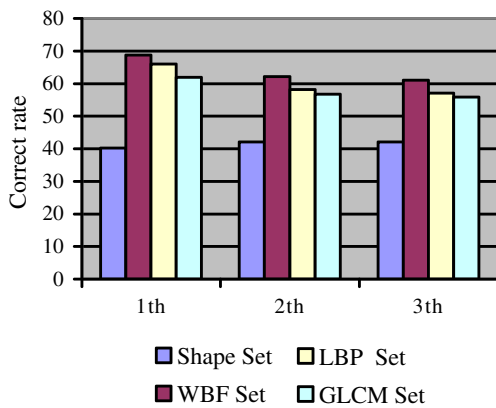


Fig. 10. Bar graph of the average correct rates of detection based on every single feature set. 1st class: normal ducts; 2nd class: contamination ducts; 3rd class: physical defect ducts.

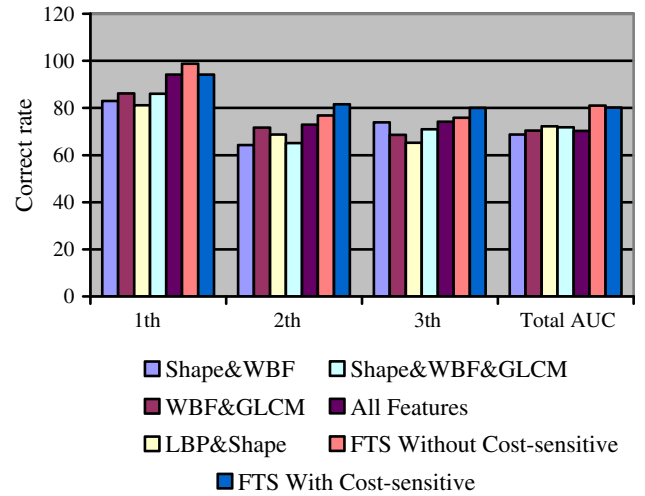


Fig. 11. Bar graph of average correct rates of detection and total AUC when using different combined feature sets and Tabu search selected feature set (FTS).

4.3.3. Detection experiments on duct inspection using different classification methods

We have applied five methods, such as k-means, seeded k-means, C4.5, SVM, and seeded k-means/C4.5, to survey duct conditions based on the features selected by Tabu search. The achieved results are listed in Table 2.

It can be seen that the correct rates of detection of k-means is lowest, while the proposed approach, seeded k-means/C4.5, has the highest correct rates. Maybe, the reasons are overfitting on high-dimensional image data sets in the clustering algorithms. The SVM based detection method has better performance of detection than other single classification methods. The duct inspection performance of combining seeded k-means and the C4.5 method using Tabu-search selected feature (FTS) is better than that of the supervised methods and anyone of the two methods.

We should note that all of the approaches in Table 2 used our method of Tabu search with cost-sensitive function to obtain the suitable parameters and features. We can regard combining k-means and C4.5 as the only reason for improving the correct rates of detection in HVAC duct inspection. We can draw a conclusion that combining k-means and C4.5 outperforms each of the two methods. The C4.5 revises decision boundaries by learning the subgroups within the cluster, relieves the two problems in clustering, i.e. the class dominance and the forced assignment problem, and improves the performance of duct inspection. At the same time the total AUC of combining k-means and C4.5 has been improved. However, there is no clear improvement of the total AUC between SVM and our proposed method.

5. Conclusions and future work

In this paper, we propose a hybrid duct detection approach by combining Tabu search and k-means/C4.5 algorithm. The seeded k-means and C4.5 are combined to improve the duct detection performance. The k-means method is first applied to partition the training instances into k disjoint clusters corresponding to the labeled seed set. The C4.5 on each cluster then refines the decision boundaries by learning the subgroups within the cluster. We introduce the cost-sensitive function into Tabu search for selecting features and construct new sample sets by using oversampling of the minority class and undersampling of the majority class to relieve the imbalance distribution of duct samples such that the most discriminating features are selected in imbalance distributions and result in higher detection accuracy of the minority class.

Future research work should be geared towards developing an effective and efficient image preprocessing method so as to further improve

Table 2
Comparison of correct rates of detection by various methods based on FTS.

Duct detection method	Correct rates of detection (%)			Total AUC
	1st class	2nd class	3rd class	
	Normal ducts	Contamination ducts	Physical defect ducts	
K-means	85.7	70.8	67.3	72.3
Seeded k-means	86.8	72.4	70.1	71.8
C4.5	88.1	73.5	69.2	71.5
SVM	94.8	76.3	78.6	80.1
Seeded k-means/C4.5	94.2	81.6	80.1	80.2

the classification performance. To explore other potential solutions, we will try to combine other methods with clustering, such as hierarchical clustering, SVM, and boosting.

References

- [1] Shanghai statistical yearbook, The seventeenth chapter—realty business, <http://www.stats-sh.gov.cn/2004shtj/tjnj/tjnj2009.htm> 2009.
- [2] B. Lundquist, et al., Assessment, cleaning and restoration of HVAC systems, http://powervac.ca/pdf/ACR_2006.pdf 2006.
- [3] H. Kuntze, H. Haffner, M. Selig, D. Schmidt, K. Janotta, M. Loh, Development of a flexible utilisable robot for intelligent sensor-based sewer inspection, Proc. of the 4th International Conference on Pipeline Construction, Hamburg, Germany, 1994, pp. 367–374.
- [4] R. Kirkham, P.D. Kearney, K.J. Rogers, PIRAT—a system for quantitative sewer pipe assessment, *Int. J. Robot. Res.* 19 (11) (2000) 1033–1053.
- [5] S.K. Sinha, P.W. Fieguth, Neuro-fuzzy network for the classification of buried pipe defects, *Autom. Constr.* 15 (1) (2006) 73–84.
- [6] O. Duran, K. Althoefer, L.D. Seneviratne, Automated pipe defect detection and categorization using camera/laser-based profiler and artificial neural network, *IEEE Trans. Autom. Sci. Eng.* 4 (1) (2007) 118–126.
- [7] M.R. Jahanshahi, S.F. Masri, Adaptive vision-based crack detection using 3D scene reconstruction for condition assessment of structures, *Autom. Constr.* 22 (3) (2012) 567–576.
- [8] Robotic inspection, cleaning and spraying system, biovac system Inc, Canada, http://www.biovacsystm.com/index.php?option=com_content&view=article&id=73&Itemid=82&lang=en.
- [9] O. Duran, K. Althoefer, L.D. Seneviratne, State of the art in sensor technologies for sewer inspection, *IEEE Sensors J.* 2 (2) (2002) 73–81.
- [10] F. Gomez, K. Althoefer, L.D. Seneviratne, An ultrasonic profiling method for sewer inspection, Proc. of IEEE International Conference on Robotics and Automation, Barcelona, Spain, April 2004, pp. 4858–4863.
- [11] D. Koo, S.T. Ariaratnam, Innovative method for assessment of underground sewer pipe condition, *Autom. Constr.* 15 (2006) 479–488.
- [12] X.H. Xie, A review of recent advances in surface defect detection using texture analysis techniques, *Electron. Lett. Comput. Vision Image Anal.* 7 (3) (2008) 1–22.
- [13] S.R. Gaddam, V.V. Phoha, K.S. Balagani, K-means + ID3: a novel method for supervised anomaly detection by cascading k-means clustering and ID3 decision tree learning methods, *IEEE Trans. Knowl. Data Eng.* 19 (3) (2007) 345–354.
- [14] Y. Ming-Der, S. Tung-Ching, Automated diagnosis of sewer pipe defects based on machine learning approaches, *Expert Syst. Appl.* 35 (2008) 1327–1337.
- [15] S. Theodoridis, K. Koutroumbas, *Pattern recognition*, 4th ed. Elsevier Inc., CA USA, 2009.
- [16] M.A. Tahir, J.E. Smith, P. Caleb-Solly, A novel feature selection based semi-supervised method for image classification, Proc. of the 6th international conference on Computer vision systems, Santorini, Greece, May 2008, pp. 484–493.
- [17] M.A. Tahir, A. Bouridane, F. Kurugollu, Simultaneous feature selection and feature weighting using hybrid Tabu search/K-nearest neighbor classifier, *Pattern Recogn. Lett.* 28 (4) (2007) 438–446.
- [18] S. Basu, A. Banerjee, R. Mooney, Semi-supervised clustering by seeding, Proc. of the 19th International Conference on Machine Learning (ICML-2002), Sydney, Australia, July 2002, pp. 19–26.
- [19] T.C. Su, M.D. Yang, T.C. Wu, J.Y. Lin, Morphological segmentation based on edge detection for sewer pipe defects on CCTV images, *Expert Syst. Appl.* 38 (10) (2011) 13094–13114.
- [20] F.T. Chan, L. Vese, Active contours without edges, *IEEE Trans. Image Process.* 10 (2) (2001) 266–277.
- [21] M. Sonka, V. Hlavac, R. Boyle, *Image processing, analysis, and machine vision*, 2nd ed. Brooks/Cole, Pacific Grove, CA, 2002.
- [22] M. Hu, Visual pattern recognition by moment invariants, *IEEE Trans. Inf. Theory* 8 (2) (1962) 179–187.
- [23] F. Luk, V. Huynh, W. North, Measurement of surface roughness by a machine vision system, *J. Phys. E: Sci. Instrum.* 22 (1989) 977–980.
- [24] J.K. Kourosh, S.Z. Hamid, Radon transform orientation estimation for rotation invariant texture analysis, *IEEE Trans. Pattern. Anal. Mach. Intell.* 27 (6) (2005) 1004–1008.
- [25] R.C. Gonzalez, R.E. Woods, *Digital Image Processing*, 2nd ed. Prentice-Hall, Upper Saddle River, NJ, 2002.
- [26] T. Ojala, M. Pietikäinen, T. Maenpää, Multiresolution gray-scale and rotation invariant texture classification with local binary patterns, *IEEE Trans. Pattern. Anal. Mach. Intell.* 24 (7) (2002) 971–987.
- [27] J.W. Cannon, J.C. Derryberry, V.Y. Kulikov, Three-dimensional data recovery using image-based modeling, Final Project Report, MIT, 2002.
- [28] G. Amal S., V. Svetha, W. Geoff, Multi-class pattern classification in imbalanced data, Proc. of International Conference on Pattern Recognition, Istanbul Turkey, August 2010, pp. 2881–2884.